[7] H. C. Cassey, Jr., B. I. Miller, and E. Pinkas, "Variation of minority-carrier diffusion length with carrier concentration in GaAs liquid-phase epitaxial layers," *J. Appl. Phys.*, vol. 44, pp. 1281–1287, Mar. 1973.
[8] J. Zucker, R. B. Lauer, and J. Schlafer, "Response time of Ge-doped (Al, Ga) As-GaAs double-heterostructure LED's," *J. Appl. Phys.*, vol. 47, pp. 2082–2084, May 1976.
[9] T. P. Lee, "Effect of junction capacitance on the rise time of LED's and on the turn-on delay of injection lasers," *Bell Syst. Tech. J.*, vol. 54, pp. 53–68, Jan. 1975.
[10] C. A. Burrus, T. P. Lee, and W. S. Holden, "Direct-modulation efficiency of LED's for optical fiber transmission applications," *Proc. IEEE* (Lett.), vol. 63, pp. 329–331, Feb. 1975.
[11] R. C. Goodfellow and A. W. Mabbitt, "Wide-band-width high radiance gallium-arsenide light emitting diodes for fiber-optic communication," *Electron. Lett.*, vol. 12, pp. 50–51, Jan. 1976.
[12] H. F. Lockwood, J. P. Wittke, and M. Ettenberg, "LED for high data rate optical communications," *Opt. Commun.*, vol. 16, pp. 193–196, Jan. 1976.
[13] A. A. Bergh and P. J. Dean, "Light-emitting diodes," *Proc. IEEE*, vol. 60, pp. 156–223, Feb. 1972.
[14] H. C. Casey, Jr., and F. A. Trumbore, "Single crystal electroluminescent materials," *Mater. Eng.*, vol. 6, pp. 69–109, 1970.
[15] H. C. Casey, Jr., D. D. Sell, and K. W. Wecht, "Concentration dependence of the absorption coefficient for n and p-type GaAs between 1.3 and 1.6 eV," *J. Appl. Phys.*, vol. 46, pp. 250–257, Jan. 1975.
[16] A. Many, Y. Goldstein, and N. B. Grover, *Semiconductor Surfaces*. New York: North-Holland, 1965, p. 260.
[17] W. Harth, J. Heinen, and W. Huber, "Influence of active-layer width on the performance of homojunction and single-heterojunction GaAs light emitting diodes," *Electron. Lett.*, vol. 11, pp. 23–24, Jan. 1975.
[18] H. Namizaki, M. Nagano, and S. Nakahara, "Frequency response of $Ga_{1-x}Al_xAs$ light-emitting diodes," *IEEE Trans. Electron Devices*, vol. 21, pp. 688–691, Nov. 1974.
[19] Y. S. Liu and D. A. Smith, "The frequency response of an amplitude-modulated GaAs luminescence diode," *Proc. IEEE* (Lett.), vol. 63, pp. 542–544, Mar. 1975.
[20] R. N. Hall, "Recombination processes in semiconductors," *Proc. IEE*, vol. 106 (Supplement), pp. 923–931, Mar. 1960.
[21] H. Namizaki, H. Kau, M. Ishii, and A. Ito, "Current dependence of spontaneous lifetimes in GaAs-AlGaAs double heterostructure lasers," *Appl. Phys. Lett.*, vol. 24, pp. 486–487, May 1974.
[22] D. L. Rode, "How much Al in the AlGaAs-GaAs laser?" *J. Appl. Phys.*, vol. 45, pp. 3887–3891, Sept. 1974.
[23] A. R. Goodwin, J. R. Peters, M. Pion, G. H. B. Thompson, and J. E. A. Whiteaway, "Threshold temperature characteristics of double heterostructure $Ga_{1-x}Al_xAs$ lasers," *J. Appl. Phys.*, vol. 46, pp. 3126–3131, July 1975.
[24] B. I. Miller, E. Pinkus, I. Hayashi, and R. J. Capik, "Reproducible liquid phase epitaxial growth of double heterostructure GaAs-$Al_xGa_{1-x}As$ laser diode," *J. Appl. Phys.*, vol. 43, pp. 2817–2826, June 1972.
[25] C. J. Hwang and J. C. Dyment, "Dependence of threshold and electron lifetime on acceptor concentration in GaAs-$Ga_{1-x}Al_xAs$ lasers," *J. Appl. Phys.*, vol. 44, pp. 3240–3244, July 1973.
[26] D. R. Ketchow, "Germanium-doped GaAs for p-type ohmic contacts," *J. Electrochem. Soc. Solid-State Sci. Tech.*, vol. 121, pp. 1237–1239, Sept. 1974.
[27] J. Stone, C. A. Burrus, A. G. Dentai, and B. I. Miller, "Nd:YAG single-crystal fiber laser," *Appl. Phys. Lett.*, vol. 29, pp. 37–39, July 1976.
[28] H. C. Casey, Jr. and F. Stern, "Concentration dependent absorption and spontaneous emission of heavily doped GaAs," *J. Appl. Phys.*, vol. 47, pp. 631–643, Feb. 1976.
[29] G. A. Acket, W. Nijam, and H. 't Lam, "Electron lifetime and diffusion constant in Ge-doped GaAs," *J. Appl. Phys.*, vol. 45, pp. 3033–3040, July 1974.
[30] C. A. Burrus, "Radiance of small area high-current-density electroluminescent diodes," *Proc. IEEE* (Lett.), vol. 60, pp. 231–232, Feb. 1972.
[31] C. A. Burrus, private communication.
[32] D. N. Payne and W. A. Gambling, "Zero material dispersion in optical fibers," *Electron. Lett.*, vol. 11, pp. 176–178, Apr. 1975.
[33] W. M. Muska, T. Li, T. P. Lee, and A. G. Dentai, "Material-dispersion-limited operation of high-bit-rate optical-fiber data links using LEDs," *Electron. Lett.*, vol. 13, pp. 605–607, Sept. 1977.

Characteristics of Integrated MOM Junctions at dc and at Optical Frequencies

MORDEHAI HEIBLUM, SHIHYUAN WANG, MEMBER, IEEE, JOHN R. WHINNERY, FELLOW, IEEE, AND T. KENNETH GUSTAFSON

Abstract—**We present a new metal-oxide-metal device (Ni-NiO-Ni, "Edge MOM") which is stable, reproducibly fabricated, and with a 10^{-10}-cm^2 tunneling area. Performing detection experiments, the device's nonlinear I-V characteristic is shown to be invariant at audio frequencies, 10.6, 3.39, and 0.6328 μm. Similar devices with 10^{-8}-cm^2 tunneling areas perform as well as the Edge MOM's in the visible and the near-infrared range, but deteriorate in performance at the 10-μm range. A dominant competing effect is a thermal-induced signal, which increases with frequency and temperature. Coupling mechanisms at the various regimes are investigated.**

The device can serve as a broad-band detector and mixer, and might in the future be a basic element of broad-band amplifiers and oscillators.

Manuscript received July 18, 1977; revised November 4, 1977. This work was supported in part by the Air Force Office of Scientific Research under Grant F44620-76-C-0100, National Aeronautics and Space Administration Grant NSG-2151, and National Science Foundation Grant ENG72-03960-A01.

The authors are with the Department of Electrical Engineering and Computer Sciences, and the Electronics Research Laboratory, University of California, Berkeley, CA 94720.

I. Introduction

We report new work on the metal-oxide-metal (MOM) device. This is one of the most interesting of recent devices, and one for which there is still much discussion about the mechanism of operation.

0018-9197/78/0300-0159$00.75

The earliest MOM device reported in the literature utilized a cat whisker tungsten wire in contact with a polished metal plate for detection of submillimeter waves [1]. The contact was not ohmic due to some trapped material at the contact, and conduction was assumed to happen by means of electrons which tunnel through this uncontrolled insulator. This particular configuration had a very small capacitance (10^{-2} pF) and a low spreading resistance (a few ohms), which led to a limiting "*RC* time constant" on the order of 10^{-13} s.

The point contact configuration was utilized in the following nine years (1966-1975) in direct detection, harmonic generation, and mixing experiments, in an attempt to find the upper frequency limit of the device. Successively, the frequency of operation was increased starting from 337 and 311 μm [2], through 118 [3], 84 [4], 78 and 28 [5], [6], 10.6 [7]-[10], 9.3 [11], 5.2 [12], 3.39 [13], [14], 3.5 and 2.2 [15], and 0.6328 μm [16]. In addition to the experiments mentioned above, the point contact configuration proved to reradiate [17] and to exhibit coupling characteristics of a linear antenna up to the 10-μm regime [18], [19]. Frequency limitation of this coupling mechanism had been predicted theoretically [20]-[22].

Unfortunately, the extreme mechanical instability of the point-contact device made it useless as a practical device, and encouraged the fabrication of a stable, integrated device. The results of only a few experiments are reported in the literature. The integrated devices so far reported are all in an evaporated form with a minimum area of 10^{-8} cm^2 (100 times larger than in the point-contact configuration). A mixing experiment at 300-μm range and direct detection up to 10-μm range was described by Small *et al.* [23]. Unfortunately, the lead resistance (400 Ω) was much larger than the tunneling resistance (50 Ω), and detected signals could as well be attributed to a combination of lead and junction thermal signals.[1] Further experiments had been carried out in the visible [24], [25]. In [24] (area 10^{-8} cm^2), the results did not show conclusively that the resulting signals were other than thermal and in [25] (area 10^{-6} cm^2), the detected signals were attributed exclusively (after the subtraction of an estimated thermal response) to photoinduced electrons traversing the barrier. Evaporated antennas (the analog to the cat whisker in the point-contact configuration) had inferior properties in the 10-μm regime, due to the high refractive index and losses of substrates and structural roughness [23], [26].

At that stage of research it was believed that the response time of the diode in its point-contact configuration was *at least* short enough to respond to signals of 2-μm wavelength. Much less was known about the evaporated structures, but it was generally believed that in the optical regime detected signals were due to photoemission effects or thermal-assisted contributions.

What are the obvious differences between the point-contact and the evaporated configurations? 1) The area of the first evaporated devices is larger by a factor of 100, 2) antennas are better (in the far infrared) in the point-contact configuration and, 3) different materials have been used in the two classes of devices.

We have decided to examine the importance of 1) and 3) using evaporated junctions with an area on the order of 10^{-10} cm^2. Mixing experiments would be more convincing, but they are much more difficult to perform in the visible, thus, we have chosen to check the devices via direct detection experiments and to use special precautions in the identification of the detected signals.

In the following sections we describe the idea behind the device operation, the method of fabrication which led to a stable device with a controlled oxide and area of $\sim 10^{-10}$ cm^2, and the results of detection experiments in 10-, 3-, and 0.6-μm ranges. All experiments were performed with large ($\sim 10^{-8}$ cm^2) and small ($\sim 10^{-10}$ cm^2) area junctions and the results led us to believe that our devices respond to the *electric field* all the way from dc up to at least 0.6 μm; namely, the response time corresponds to frequencies which are at least in the visible range.

II. Principles of Operation

We first consider an ideal model. A thin crystalline insulator that is sandwiched between two parallel faces of ideal conductors, can be represented in an energy diagram representation as a potential barrier (its height is some fraction of the energy gap of the insulator) for electrons which are concentrated near the Fermi levels of both conductors.

If a potential difference is generated between the two conductors, a net number of electrons can traverse the barrier via thermal excitation above the barrier (Schottky emission) and by tunneling through the barrier. For example, under low biasing conditions and at room temperatures, for a 10-Å barrier thickness and a barrier height greater than 0.1 eV, the tunneling current will be dominant. In the tunneling regime, if a simple model is assumed, a small biasing voltage $V(\text{eV} << \Phi)$ will result with a tunneling current of the form

$$I = cAV \exp - b\Phi^{1/2} d \tag{1}$$

where Φ is the barrier height, d is the oxide thickness, A is the area, and b and c are constants. For example, if $A = 10^{-10}$ cm^2, $d = 7$ Å, and $\Phi = 2$ eV, the zero bias dynamic resistivity r_d is about 100 Ω; for $d = 15$ Å and $\Phi = 0.5$ eV, $r_d \sim 5$ kΩ. These numbers will give us some idea of the oxide thickness in our devices. The resulting I-V characteristic is nonlinear, and its details depend on the metals and insulator types, and insulator thickness.[2] For detailed tunneling equations the reader should refer to [27] and to the references contained in it. The tunneling electrons traverse a 10-Å thick barrier in times as short as 10^{-15} s [28], [29], hence, it is reasonable to believe

[1]We detected similar signals all the way into the visible on similar junctions and found a good correlation with simple thermal contributions.

[2]The "real" junctions are far from being ideal. For example, if d = 10 Å, the number of surface states exceeds the number of bulk states and energy bands are allowed in the gap, the transition from oxide to metal is not abrupt, the fluctuations in the oxide thickness are probably as large as the oxide thickness, image corrections will vary the barrier shape, and more. No attempt is made to compare results with theory, but tunneling will be assumed to be the dominant phenomenon of conduction.

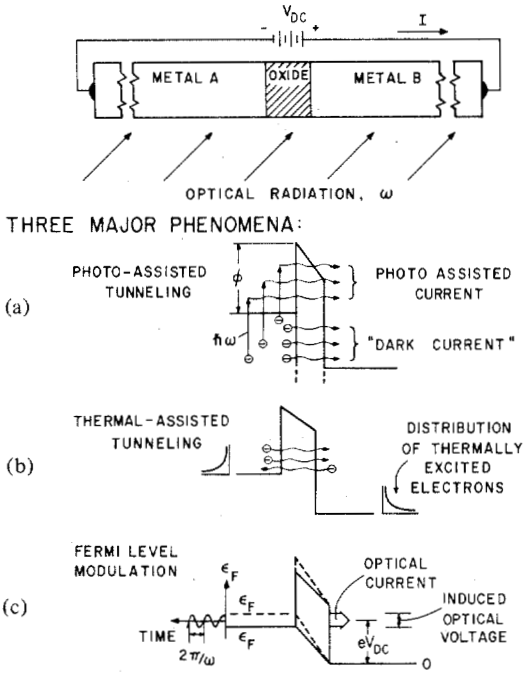

Fig. 1. Three major phenomena result when radiation is shined on a biased junction. (a) Photo-assisted tunneling. "Dark current" is due to the electrons that are not excited. For simplicity, electron excitations in only one metal are shown. (b) Thermal-assisted tunneling. The Fermi tails are only of the order of KT. (c) Fermi level modulation around the biasing point eV_{dc}. The potential barrier is simplified by a trapezoidal barrier.

that the dc I-V characteristic is invariant up to at least 10^{15} Hz (the visible range). In the visible range the "RC time-constant" concept has to be examined carefully [22], since its validity will affect the magnitude of the optical voltage across the junction.

When optical radiation impinges on a biased junction, at least three major phenomena take place (they are described pictorially in Fig. 1).

A. Photo-Assisted Tunneling

Electrons in the metals, in the vicinity of the barrier, absorb photons and gain energy $\hbar\omega$. The excited electrons tunnel with larger probabilities or surmount the barrier. It is believed that the barrier height is bias dependent [27], so this contribution should monotonically increase with bias [25]. An open-circuit voltage across the junction will result from an opposite current that flows through the junction[3] [25]

$$V_{PA} = -I_{PA} r_d$$
$$I_{PA} = b[\hbar\omega - \Phi(V_b)]^2 \tag{2}$$

where V_{PA} and I_{PA} are the photo-assisted voltage and current in the junction, $\Phi(V_b)$ is the bias dependent barrier height, and b is a constant proportional to the area of the junction.

The effect is *inherently fast*[4] and depends linearily on the area of the junction. Since the highest quantum yield which had been reported did not exceed 0.1 percent [31], [32], and our devices possess a very small area (10^{-10} - 10^{-8} cm^2), the induced photo-assisted open-circuit voltage is much smaller than the other two phenomena to be described.[5]

B. Thermal-Assisted Tunneling

The incoming photons are coupled to phonons and the metal's temperature rises. Fermi electrons will gain $\sim K\Delta T$ additional energy—according to the Fermi-Dirac distribution—and the tunneling current will increase. When the preirradiation temperature of the device is lower, for the same ΔT, less current will be induced, an obvious consequence of tunneling probability versus energy relations. This effect is *inherently slow*[6] and is not directly related to the junction area. As a result of our experiments, we have observed that the open-circuit thermal-assisted signal increases monotonically with bias.

C. Field-Assisted Tunneling (or Fermi-Level Modulation)

By some coupling mechanism (antenna in the far infrared [18], [19], surface plasmons or other in the visible [22]), an electric field is enhanced in the barrier, and since $d << \lambda$, an "optical-voltage" can be defined. This voltage will alternate at the applied frequency (ω) around the quiescent point (V_{dc}), and will enhance an ac current component in addition to the existing dc current bias (via the modulation of the Fermi levels in both metals—one with respect to the other).[7] Due to the nonlinearity of the I-V characteristic, a dc, 2ω, $3\omega \cdots n\omega$ frequency components will be generated. Provided the I-V characteristic is invariant from dc up to $n\omega$ and the applied ac signal is small enough, the nth frequency component will be related to d^nI/dV^n of the dc I-V characteristic. In particular, the open-circuit dc voltage across the junction will be

$$V'_{dc} = -\frac{1}{4}\frac{I''}{I'} V_{ac}^2|_{V_{dc}} \tag{3}$$

where $I'' \equiv d^2 I/dV^2$, $I' \equiv dI/dV$ (we will define "sensitivity" as $S \equiv -I''/I'$), V_{ac} is the amplitude of the ac voltage across the junction, and V'_{dc} is the dc contribution at the biasing point V_{dc} (marked as $|_{V_{dc}}$). The area of the junction, its geometrical configuration and the properties of the radiating source determine V_{ac}. As will be shown later, the field contribution is greater at lower temperatures, due to an enhancement in I''/I'. Fig. 2 describes graphically the generation of an open-circuit dc signal at two different temperatures.

As was mentioned earlier, the MOM in its point-contact configuration gave the best experimental results, but its instability was a major drawback. On the other hand the "large

[3]The opposite current is necessary to satisfy open-circuit conditions. r_d is used assuming ac techniques employed.

[4]The time is limited by the excitation and transverse times of electrons, both in the 10^{-15}-s range or less.

[5]For a 0.6328 μm, 1-mW laser, focused into a 25-μm spot, and assuming 30 percent of incoming light absorbed in the metals of a junction, the photo-assisted signal is estimated to be a function of 1 μV and much less for longer wavelengths.

[6]Limited by the thermal time constant of the junction (heat conductivity and geometrical effects). Experimentally found to be around 50 μs.

[7]This change of potential energy of the metals is probably due to an accumulation of charges on the surface of the metals (limited by the relaxation times in the metals, which are also on the order of 10^{-15} s [30]).

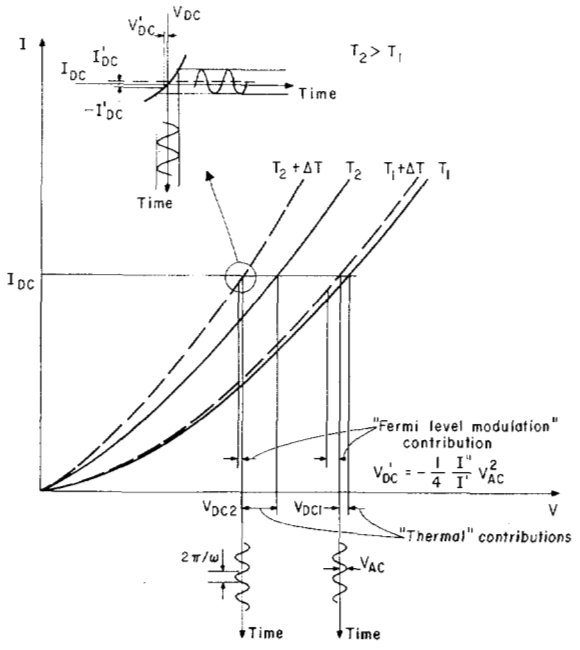

Fig. 2. Thermal and field contributions. When radiation impinges on junction an ΔT change in junction temperature arises and the I-V characteristic is modified. Note the significant reduction in the thermal contribution when the temperature is decreased. The generation of V'_{dc} is shown. Assuming V_{ac} is applied by a voltage source, the optical current is a distorted sine wave with a dc component I'_{dc}. $-I'_{dc}$ flows to keep I_{dc} constant (open circuit condition) and $-V'_{dc}$ is generated.

area" evaporated junctions did not give satisfactory results, probably due to the differences in geometrical structure, area and the choice of metals and substrates. In the next section we describe the fabrication and structure of a new device: the "Edge-MOM" junction that solves the "area" problem—employing simple fabrication methods—and introduces a number of new possibilities in the exploitation of MOM junctions.

III. The Fabrication of "Edge-MOM" Junction

At first we attempted to fabricate 1 μm × 1 μm junctions composed of Al-Al_2O_3-Al. Aluminum seemed attractive at the time because of its high reflectivity over a wide range of frequencies (which would have reduced thermal and photon assisted effects), its low dc resistivity, and the vast amount of data in the literature on Al-Al_2O_3-Al junctions (see, for example, [33], [34]).

Since aluminum tends to oxidize easily, the resulting oxide was very sensitive to many uncontrolled parameters, and the fabrication of junctions in the kilohm range was not reproducible. After testing a few of the aluminum junctions at near-infrared and visible frequencies, we realized that the thermal signal was dominant (even at 77 K), and if the field induced signal existed, it was too small to be detected. We also realized that the nonlinearity of the I-V characteristic was very small, and $S \equiv -I''/I' \lesssim 0.1$ (much less than in the point-contact junctions which had $S \cong 10$. See also [25] for S value).[8] Since S was small and the area was large in the

[8]Probably due to high $\Phi(\sim 2$ eV) and the very small $d(5-10$ Å), the I-V curve has an ohmic nature.

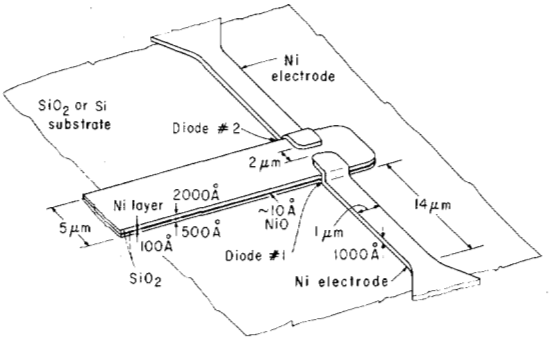

Fig. 3. Schematic description of the "Edge-MOM" device. Each Ni electrode serves as a long antenna in the infrared and is terminated with a junction. Central pad is extended in its shape to allow an electrical contact in the purpose of shorting a single junction by a voltage pulse.

aluminum junctions, an unavoidable conclusion was reached: to look for a junction with an enhanced nonlinearity, which could be reproducibly fabricated and preferably with an area of $\sim 10^{-10}$ cm^2.

An overlap of two 0.1-μM metal strips would give the desirable area, but conventional photolithographic techniques do not have sufficient resolution, and "electron-microscope exposure" techniques are not efficient for the fabrication of a large number of junctions on one chip at this time. We have developed a method that involves an overlap between a 1-μm metal strip and an oxidized edge of a metal strip, ~100 Å thick, to get an overlap area of 1 μm × 100 Å = 10^{-10} cm^2. We named the new junction an "Edge-MOM" junction. A device of this kind can be fabricated using conventional fabrication techniques. Since one of the metal electrodes is only 100 Å thick, the resulting lead resistance is 100-200 Ω. To overcome this problem we fabricated the device which is described in Fig. 3. Two junctions separated by 3-5 μm exist in one device. The biasing current flows through the two thick electrodes (1000 Å thick), and only through a 3-5-μm path, in the thin metal film. As a result, the lead resistance is reduced to 10-40 Ω. The two electrodes (1 μm in width) serve also as two antennas in the infrared regime; each antenna is terminated by a tunneling junction. On top of the 100-Å nickel layer, a thick insulator is deposited (SiO_2), to eliminate tunneling through these overlapping areas.

By a process of trial and error,[9] we found that nickel-nickel oxide-nickel junctions can be reproducibly fabricated and have S on the order of 1-10.

Let us first describe the method of oxidation, which has been the key for the successful fabrication of the junction. We have adopted an oxidation procedure which was developed by Greiner [35]. The method involves sputter etching and oxidation processes simultaneously. As is well known, the rate of oxidation decreases when the oxide thickness increases following the logarithmic law [35]: $(dx/dt)_{\text{oxidation}} = Ke^{-x/x_0}$,

[9]We have used silver, copper, gold, chromium and nickel. Silver, copper and chromium oxidized too readily and the silver film deteriorated in time. Chromium had a high dc resistance. Gold could not be oxidized. Ni-NiO-Al and Ni-NiO-Au were unstable electrically, (probably due to ion migration between the different metals).

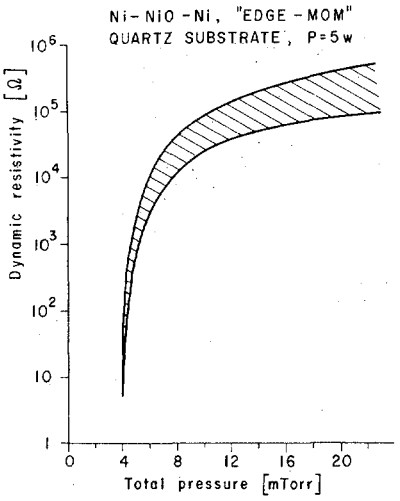

Fig. 4. A calibration curve for Ni–NiO–Ni "Edge MOM." The dynamic resistivity is measured at zero bias, for a single junction. The gas mixture is Ar(80 percent) - O_2(20 percent) and the power is kept constant at 5 W (corresponding to an accelerating voltage ~80 V dc). The substrate is quartz. (For Si substrate the resistivities are somewhat lower, presumably due to the larger heat conduction of the Si and the resulting lower temperature during oxidation).

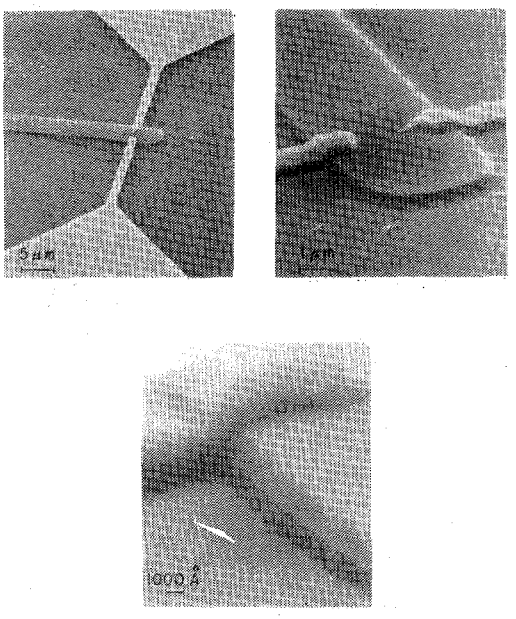

Fig. 5. SEM photographs of the final device. Note the 100 Å of nickel layer clearly seen sandwiched between the quartz substrate and the sputter-deposited SiO_2. Note too, the unavoidable roughness of the nickel electrodes due to the chemical etching. (Tilt angle 45°.)

where K and x_0 are oxidation parameters and x is the oxide thickness. The sputter-etching rate can be assumed a constant R. If the parameters are chosen so that the initial rate of oxidation is higher than the sputtering rate, oxide will grow asymptotically to $x_{\text{final}} = x_0 \ln K/R$ with a time constant x_0/R. If $t >> x_0/R$, both rates—oxidation and sputtering—are equal, and the process afterwards is time independent.[10] Moreover, a prolonged process will improve the quality of the oxide due to a reduction in the number of oxide pin-holes.

Oxidation and etching parameters that can be controlled are: partial pressure of oxygen in an argon plasma, total pressure of the oxygen-argon mixture, accelerating dc voltage and substrate temperature.[11]

The oxidation was performed in a multitarget RF sputtering unit.[12] To minimize changes in the substrate temperature, the substrate utilized a heat sink of gallium to a water cooled substrate holder, and the oxide thickness was controlled by changing the total pressure of a mixture argon (80 percent)-oxygen (20 percent), without changing the accelerating voltage and the partial pressure of oxygen.[13] A calibration curve of the zero-bias dynamic-resistance versus total pressure for the "Edge MOM" is given in Fig. 4. The results were fairly reproducible from run to run, and all diodes on the same substrate did not vary by more than 2:1 in their dynamic resistances.

Junctions have been fabricated on two different substrates. For experiments using radiation with wavelengths 0.6328 and 3.39 μm, a quartz substrate was used, and for a 10.6-μm wavelength, a silicon substrate (n type, ~5 $\Omega \cdot$ cm) with some 500 Å of SiO_2 for dc isolation was used.[14] Metals and dielectrics were sputter-deposited in a multitarget RF sputtering unit.[12]

After the deposition of some 100 Å of nickel layer, and 2000 Å of SiO_2 on its top (without breaking the vacuum), the substrate was removed from the system, and the shape of the first electrode was formed lithographically with positive photoresist (~3–5 μm wide). Baking for two hours with a gradual increase in temperature up to 160°C hardened the photoresist, which served as a mask in a successive sputter-etching procedure.[15] The sputter etching removed the unmasked top SiO_2, the 100 Å of nickel layer, and 500 Å of the SiO_2 substrate, leaving the edge of the nickel layer exposed. The hardened photoresist was removed in an oxygen plasma-asher. The substrate was then introduced back into the multi-target sputtering unit, and the system was evacuated to 10^{-7}-torr range. First, sputter etching was performed (with pure argon), to remove oxide that grew on the nickel layer edge, and then oxidation was performed for 10 min following the procedure described above. The system was evacuated again and ~1000 Å of nickel was sputter deposited.[16] After removing the substrate, a photoresist pattern of the top electrodes (1 μm in width) had been formed photolithographically,

[10]Two minutes is a typical time constant, and 10–15 minutes is the actual time used for growing a ~15-Å oxide.

[11]Practically, it is very difficult to control the temperature, and this parameter leads to some spread in the results.

[12]NRC 836 (Randex), by Perkin-Elmer. 5-in target diameter, 2.5-in target-substrate holder separation.

[13]The acceleration voltage was 80–100 V (~5-W incoming power), and the total pressure was controlled in the range 5–20 mtorr.

[14]For the λ = 0.6328- and 3.39-μm ranges, sapphire substrates were tried too, but they could not be purchased scratch free. For the λ = 10.6-μm range CaF_2 was evaporated and MgO was sputtered on top of the Si substrate, in order to replace the very lossy SiO_2. The CaF_2 after evaporation had a rough surface and the MgO was etched away by all etchants for the metals. A CaF_2 substrate was tried too, unsuccessfully.

[15]In a sputtering unit by Vacuum Technology Associated (VTA), 5-in substrate diameter, 4-in substrate-anode separation.

[16]This is a critical point. In the time interval between the end of oxidation and the deposition of the top nickel electrode, the nickel edge can be continuously oxidized thermally, from residual of oxygen in the system. This time interval was reduced to 90–120 s, and that included the time needed to clean the nickel-oxide from the top of the nickel target before deposition.

and the top nickel layer had been etched chemically down to the substrate, forming the "Edge-MOM" device. The photoresist was then removed chemically. The final product is shown by the SEM pictures in Fig. 5.

Edge MOM's with zero-bias dynamic resistivities beginning from 100 Ω and up to 1 MΩ and above, were fabricated reproducibly. The I-V characteristics were very stable and did not change after many cycles of biasing. Slight aging, resulting in the increase of the diode resistivity, occurred over days. To minimize the aging effect, each diode was formed immediately prior to its use (by etching the top metal structure and removing the photoresist mask).

Large area MOM's (~1 μm^2) were prepared simultaneously with the Edge MOM's. The only structural difference was the absence of the top SiO_2 buffer so that the tunneling area in each junction was 1 μm × 1 μm = 10^{-8} cm^2.

It seems appropriate now to describe shortly the difficulties we faced in handling the devices and the experimental setup which we employed for the detection experiments.

IV. Device Handling and Experimental Setup

A 0.1 V across the junction will be sufficient to develop an electric field in the range of 10^6 V/cm in the oxide. Since the oxide is probably not extremely pure, the breakdown fields are smaller than in a pure bulk material. As a result, the device is very vulnerable to an accumulation of static charges, transients from the line, and pick-ups of low-frequency voltage from surrounding equipment (especially when leads are connected to the electrodes). The "statics" problem was the major one, and a vast number of junctions turned into shorts without any apparent reason, even though all precautions had been taken. We have succeeded in controlling the problem only by raising the relative humidity in the laboratory to about 60 percent. The other problems were controlled by using a complete differential setup where all the outer coaxial shields were grounded. Gold wire leads were connected via silver paint using wooden sticks, and the junction was shorted with a variable resistor before and after each step of the experiment. The device was mounted in a metallic grounded Dewar which enabled us to cool it down and to shield it from electrical pick-ups.

When all precautions were taken, the device had an indefinitely long lifetime, except for a slight aging which resulted in the increase of its resistivity. Experiments were performed on a single junction[17] at room temperature and at liquid-nitrogen temperature.

First, the quasi-dc I′ and I″ were monitored as a function of the dc biasing voltage, which was supplied by variable current source. I″ was monitored by mixing two low-frequency signals (40 and 42 kHz, 10 mV each) supplied by a voltage source (54-Ω output impedance). The frequency difference (2 kHz) was monitored using a lock-in amplifier (LIA).[18]

[17]One of the two adjacent junctions had been burned by a voltage pulse, which had resulted in its shorting. The connection to the outer circuit had been done via the two 1000-Å thick nickel electrodes.

[18]PAR lock-in amplifier, model 124; with a differential preamplifier, Model 116 (110-MΩ input impedance).

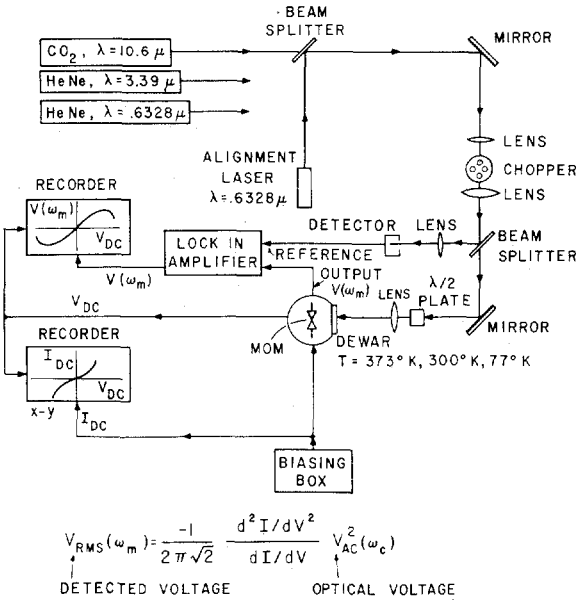

Fig. 6. Schematic description of the experimental setup. The equipment for measuring I′ and I″ are not shown in the figure.

I′ was established from dynamic resistivity measurements. For the detection experiments (Fig. 6), three different lasers (λ = 0.6328, 3.39, and 10.6 μm) were focused (by a 5-cm CaF_2 lens), on a chopper (930 Hz), to generate an almost ideal square-wave modulation (with rise times of 2 μs in the visible, 10 μs at 10.6 μm). The beams were then collimated (by a 10-cm NaCl lens), passed through a λ/2 plate, and focused (by a 10-cm CaF_2 lens) onto the diode which was placed inside a Dewar, with a ZnSn window. The output signal from the diode was monitored by the LIA,[18] which was synchronized to a reference signal generated by a collinearized alignment laser. The junction's dc current and the LIA's output were displayed by two x-y recorders simultaneously, as a function of the biasing voltage.

The detected signal is then compared qualitatively with the predicted thermal and field induced signals. The thermal signal can be deduced by the change of the I-V characteristic versus temperature (see Fig. 2), and after subtraction, the remaining part $V(\omega_m)$ will be compared with

$$V_{\mathrm{rms}}(\omega_m)\Big|_{V_{\mathrm{dc}}} = -\frac{1}{\sqrt{2\pi}} V_{\mathrm{rms}}^2(\omega_c) \frac{I''}{I'}\Big|_{V_{\mathrm{dc}}} \tag{4}$$

where $V_{\mathrm{rms}}(\omega_m)$ is the rms value of the first harmonic at the chopping frequency (ω_m = 930 Hz) and $V_{\mathrm{rms}}(\omega_c) = 1/\sqrt{2}$ $V_{\mathrm{ac}}(\omega_c)$, where V_{ac} is the amplitude of the optical voltage which is developed across the junction and is assumed to be constant. The electric field available from the lasers is found by:

$$\frac{P}{A} = \frac{E_{a,\mathrm{rms}}^2(\omega_c)}{\eta} \tag{5}$$

where P is the laser power, A is the effective focal area, $E_{a,\mathrm{rms}}(\omega_c)$ is the rms electric field in the focal point, and η is the characteristic impedance of the ambient in which the junction is immersed in (η = 377 Ω will be used). The optical

voltage available across the junction $V_{a,\,\mathrm{rms}}(\omega_c)$ can be estimated by

$$V_{a,\,\mathrm{rms}}(\omega_c) = E_{a,\,\mathrm{rms}}(\omega_c)\, d \tag{6}$$

where d is the oxide thickness (10 Å will be used). An "enhancement factor" G will be calculated via the definition

$$G = \frac{V_{\mathrm{rms}}(\omega_c)}{V_{a,\,\mathrm{rms}}(\omega_c)} \tag{7}$$

G can give some clue on the coupling mechanism.

The experimental results which are described in the following section will help us to determine whether the dc I-V characteristic is valid at optical frequencies, the relative importance of "thermal" and "field" contributions, and the importance of area. Also, we will get some idea about the coupling mechanism and the noise characteristics of the device.

V. Experimental Results

Experiments have been carried out on four types of junctions: "Edge" and large-area MOM's on quartz and silicon substrates. The success of our experiments depended strongly on the detailed shape of I''/I' and the magnitude of the thermal-assisted signal relative to the field-assisted signal. Unfortunately, thin nickel films (100–200 Å) absorb around 40, 20, and 10 percent of the incident power at $\lambda = 0.6328$, $\lambda = 3.39$, and $\lambda = 10.6$ μm, respectively, which leads to a large thermal contribution that is dominant at the optical frequencies. But, fortunately, as a compensation for the low reflectivity of nickel, the sensitivity S of Ni-NiO-Ni junction, is quite high, and has a distinct peak which occurs around a biasing voltage of 100 mV. This peak becomes even more profound at lower temperatures, and when the temperature is reduced even more, another peak shows up at ~150 mV.[19] If upon shining radiations with different wavelength on our device, the detailed structure of I''/I' versus V_{dc} is reproduced, it will suggest that mixing of sidebands occurs at the frequency of the radiation, and optical currents are flowing through the junction at this frequency.

Let us begin with results, when 10.6-μm wavelength was used. Fig. 7 describes typical I-V and $-I''/I'$ curves of a *large-area* single junction at 300 K and 77 K, fabricated on top of a Si substrate (covered with ~500 Å of SiO_2).[20] $-I''/I'$ results from two separate quasi dc measurements; $1/I'$ [Fig. 8(a)] and $-I''$ [Fig. 8(b)]. Note that I'' at 77 K changes very little relative to I'' at 300 K, but I' has a threefold change which leads to a similar enhancement in $-I''/I'$. As a result of Fig. 7, we hope to get a larger field-assisted contribution at lower temperatures [see (4)]. When 10.6-μm radiation was

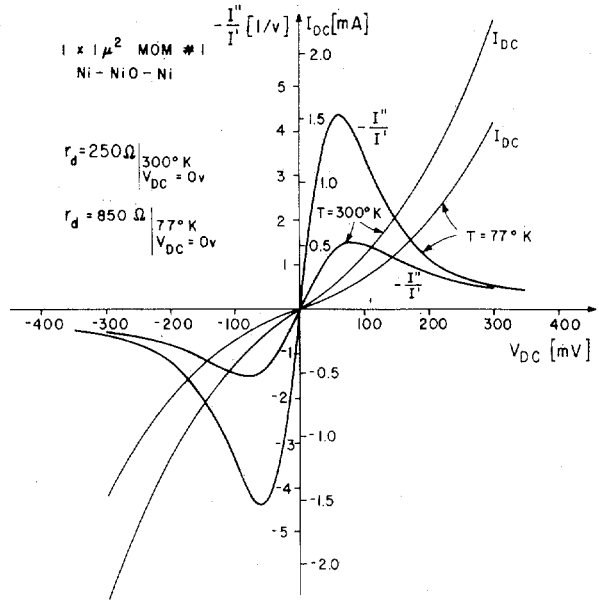

Fig. 7. Characteristics of a large-area single MOM (no. 1) at two different temperatures. Junction characteristics are antisymmetric. Spreading resistivity is about 10 Ω.

focused onto the junction (about 100 mW, 150-μm focal spot), the signals shown in Fig. 9 were detected by the LIA (plotted for positive bias only). We have also plotted the expected thermal signal that was deduced from Fig. 7 (see Fig. 2 for the method), and the two curves agree rather well (the interpolated signal was needed to match $V(\omega_m)$ at its maximum). Apparently the detected signal at room temperature is mostly thermal. When the device was cooled down the thermal signal dropped considerably (5 to 10 times), and the field-assisted contribution—that was predicted to be enhanced threefold—showed up from the background of the thermal contribution. If the thermal signal is interpolated and subtracted out from the total detected signal at 77 K [Fig. 10(a)], the field contribution remains ($V(\omega_m)$), as shown in Fig. 10(b).[21] For comparison, $-I''/I'$ is plotted too, and the agreement between the curves is very good. The results above will provide us with the enhancement factor G(7), as will be discussed in the next chapter. Apparently the junction, even though its area is 10^{-8} cm^2 and its calculated time constant is around 10^{-11} s, seems to respond to the 10.6-μm wavelength and as we will soon see, all the way to at least 0.6-μm range.

Similar quasi-dc characteristics have been observed when an "*Edge-MOM*" was tested ("Edge-MOM" no. 2, Fig. 11). In this particular junction, the second-peak in I'' (near 150 mV) is more profound when the dc bias is positive (1000-Å Ni positive with respect to oxidized 100-Å Ni). When the CO_2 radiation is focused on the device, an enhancement in the field-assisted signal is clearly seen—even at room temperature—comparatively to the signal from the large-area junction. At 77 K the detected signal has a very distinct peak near $V_{\mathrm{dc}} = 80$ mV and the estimated thermal contribution is assumed to

[19] The first peak appears also in Al-Al_2O_3-Al junctions but in a less profound form. Although we are not certain of the physical reasons for the peaks, we can suggest some possibilities: 1) a result of the energy band structure of nickel, 2) a result of the overall tunneling equations including all parameters such as fluctuation in oxide thickness, field penetration into electrodes, surface states, traps, etc., and 3) inelastic scattering in the oxide due to trapped molecules. Peaks like these had been shown to exist by Lambe and Jaklevic [36].

[20] I-V, I'-V and I''-V are monitored when the radiation is focused on the junction to maintain the actual temperature that exists in the detection experiment.

[21] The thermal signal was interpolated so that its subtraction will fit I''/I' around $V_{\mathrm{dc}} = 300$ mV (an inaccuracy in the interpolation would not change the shape of $V(\omega_m)$ considerably).

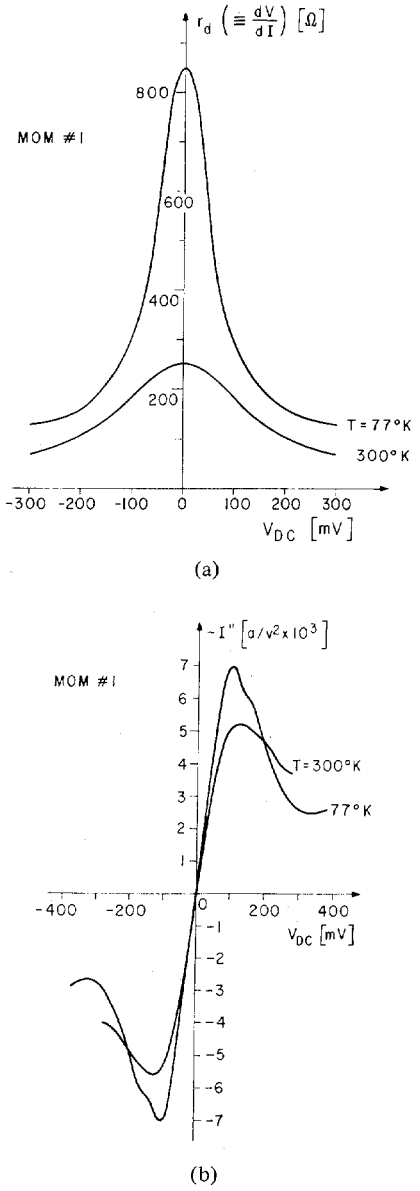

Fig. 8. Large-area MOM (no. 1). (a) Dynamic resistivity versus V_{dc}. (b) d^2I/dV^2 versus V_{dc}. Note a second peak that starts showing up at V_{dc} = 150 mV.

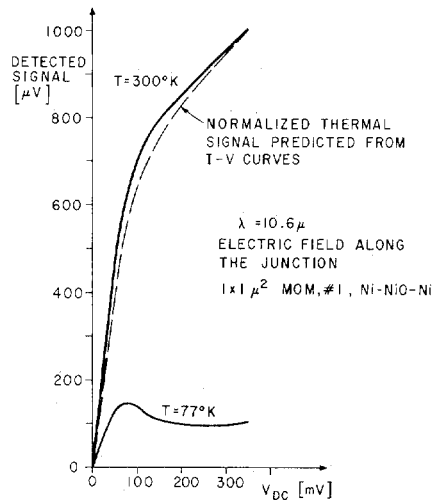

Fig. 9. Detected signals for $\lambda = 10.6$ μm at $T = 300$ K and $T = 77$ K. Field is polarized to accelerate electrons across the oxide ($\vec{E}_\parallel$). Thermal signal drops, and a distinct peak appears at low temperatures. At room temperatures, the thermal signal is dominant.

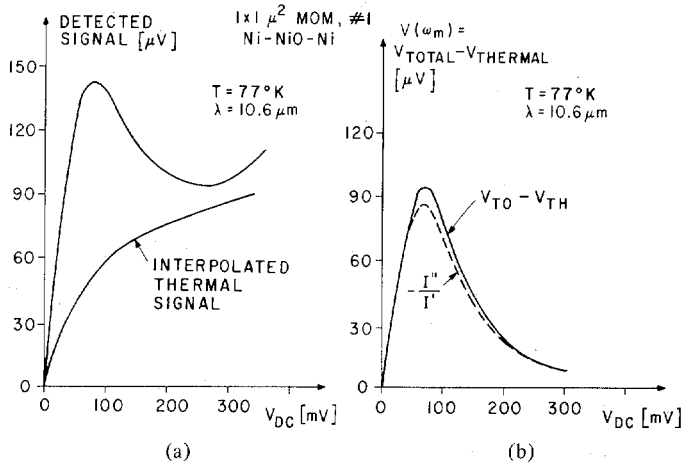

Fig. 10. Description of obtaining the field-assisted signal. (a) Detected and interpolated thermal signals. (b) A qualitative comparison between $V(\omega_m)$ and $-I''/I'$.

be reduced by approximately six times from the one at 300 K (Fig. 12). We did not bother to subtract the thermal signal in Fig. 12 (that will make $V(\omega_m)$ and $-I''/I'$ very much alike) since the resemblance is striking even when it is included.

Antenna properties of the configuration had been checked via polarization and angle dependence. When $\vec{E} = \vec{E}_\parallel$ (Fig. 12), the field contribution is enhanced more than five times with respect to the case where $\vec{E} = \vec{E}_\perp$ for $\theta \geqslant 45°$, and more than four times at normal incident. Also the shape of the curve is more like $-I''/I'$ when $\vec{E} = \vec{E}_\parallel$. This agrees rather well with the assertion of "Fermi levels modulation" which implies that a field along the propagation path of electrons in the oxide is necessary. When the angle θ is changed, an antenna enhancement or lobe structure is not observed, but without much surprise since the structure has rough edges from the chemical etching (see Fig. 5) and both the SiO_2 layer on the silicon and the sputtered nickel are lossy.[14] The high index of refraction of silicon (~3), causes a large reflection and reduces the field at the interface, especially at large θ, where the antenna enhancement should be the largest.

But note that with change of angle, the ratio between the two contributions ($\vec{E}_\parallel$ and $\vec{E}_\perp$) is enhanced, since the thermal signal drops fairly fast with angle but not so the field contribution, probably due to some enhancement of the "antenna-structure."

Experiments have also been carried out with large area and Edge-MOM's (both fabricated under the same conditions on quartz substrates), employing radiation at 3.39- and 0.6328-μm wavelengths. As expected, the thermal signals were stronger than in the 10-μm range, but to our surprise, no significant difference in the enhancement factor G was observed in the edge junctions. We offer a possible explanation in the next section.

The quasi-dc I' and I'' versus V_{dc} of these junctions are very similar to the previous junctions and are not shown here. The

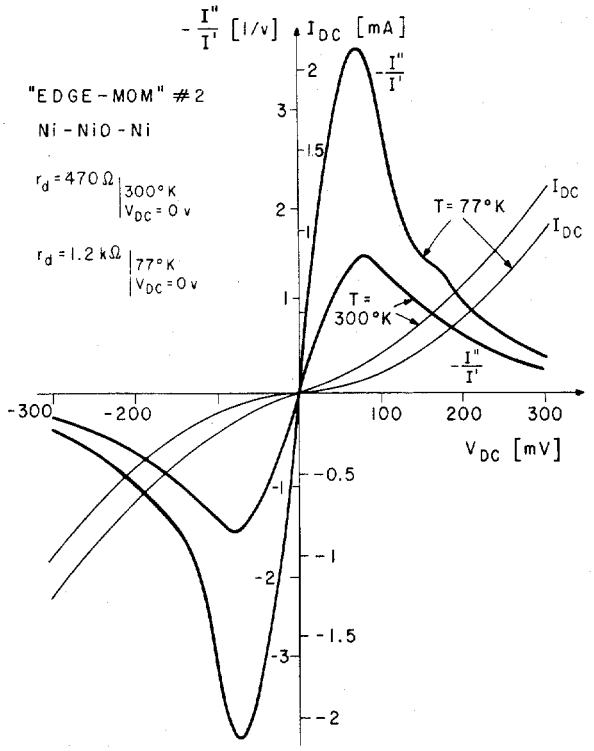

Fig. 11. The dc I-V and Quasi-dc I″/I′ of "Edge-MOM" no. 2. A distinct second peak appears in I″ for $V_{dc} > 0$ (less apparent in $-I''/I'$).

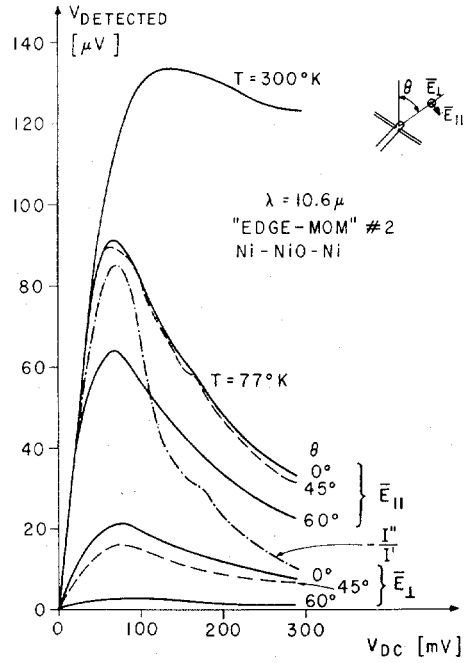

Fig. 12. Detected signals from a single "Edge-MOM." Thermal- and field-assisted signals are on the same order of magnitude even at room temperature. Note, the slight "bump" in $-I''/I'$ (near V_{dc} = 150 mV), that is reproduced in the detected curves.

detected signals at the output of the large area and edge diodes are very much alike in shape and amplitude and are plotted in Fig. 13 (0.6328 μm at 1 mW and 50-μm focal spot, 3.39 μm at 1 mW and 100-μm focal spot). The signals are normalized so that at T = 300 K, $V_{DET.}$ (0.6328 μm) and $V_{DET.}$ (3.39 μm)

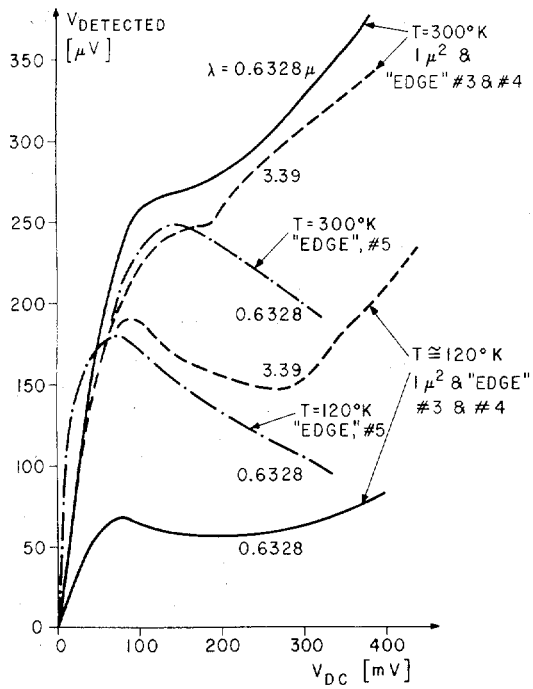

Fig. 13. 3.39- and 0.6328-μm detection results, on large-area and Edge-MOM's. Junctions no. 3 and 4 had been fabricated simultaneously. The familiar peak near V_{dc} = 100 mV shows up at the output of junctions no. 3 and 4 for $T \cong 120$ K and dominant at the output of junction no. 5, even at T = 300 K (λ = 0.6328 μm).

will be similar in magnitude for junctions no. 3 and 4.[22] It is clearly seen that the amount of thermal signal is larger at 0.6-μm range than at the 3-μm range and upon cooling down, the field-assisted signal shows up with the familiar peak.[23] We did not subtract in Fig. 12 the interpolated thermal signal, but again, its subtraction led to a very good agreement between $-I''/I'$ and $V(\omega_m)$.

Another junction that was fabricated in a different run (no. 5), which had a smaller dynamic resistivity (~500 Ω), produced a field-to-thermal signal ratio that was much better even in the 0.6-μm regime, and we have plotted the detected signals in Fig. 13. In general, lower impedance junctions had less thermal contributions than the high impedance ones, and so, even weak field-assisted signals could be seen rather easily at their output terminals. Polarization dependence was not profound in the 3 and 0.6 μm ranges.[24] No quantitative measurements of noise had been carried out. The noise increased with biasing, and best signal-to-noise ratio occurred at the peak of the detected signal near V_{dc} = 100 mV.

In the next section we analyze the results and summarize them.

[22] Light was shined from the back of the substrate to have a clear approach to the junction, which is buried under 1000-A thick nickel electrode.

[23] Due to the low heat conductivity of the quartz substrate, the temperature of the junction was estimated to be ~120 K (and not 77 K). This led to a larger thermal signal than could have been achieved at 77 K.

[24] *Note added in proofs:* Recent experiments with junctions fabricated on sapphire resulted in undetectable signals at the 0.6 μM range. We tend to believe at the moment that the previously detected signals at 0.6 μM range were pure thermal signals due to the poor heat conductivity of the quartz substrate. Experiments are planned with higher power lasers.

VI. Discussion and Concluding Remarks

When the detected signals (after the subtraction of the thermal contribution) are compared with $-I''/I'$, the distinct feature in both (the peak near $V_{dc} = 100$ mV) helps to conclude that they must result from a rectification of optical currents by the nonlinear I-V characteristic, which must be invariant (to the degree of accuracy of the results) up to at least the frequency of the optical currents.

Using (4)-(7), laser power and beam spot measurements, and exact geometrical configurations, Table I is constructed. From it we see that in the 10-μm regime the "Edge MOM" has the largest G. At higher frequencies G drops and no difference is observed between the two classes of MOM's.

What can we say about the coupling mechanism at the three wavelengths which we have used?

In the 10-μm regime the agreement of $V(\omega_m)$ with (4) suggests a "voltage source" type of coupling, which can be justified assuming some type of antenna coupling (with radiation resistance of 100 Ω or less [9], [19]). This assumption is strengthened by the strong polarization dependence and the large enhancement factor (70-150).

In the 3- and 0.6-μm regimes, enhancement in the range of 10-20 can be explained theoretically by a simple match of electric fields at the boundary of the metal-oxide interface. The electric field can be evaluated inside the metal, and then, by using the continuity of normal $\epsilon\vec{E}$ components to the junction interface: $E_{oxide} = E_{metal}\ |\epsilon_{metal}/\epsilon_{oxide}|$. The resultant E_{oxide}/E_a [see (5)] is in the 10-20 range. Coupling assumptions like that or via surface plasmons [22] are pretty much independent of d, hence, a "voltage source" coupling type assumption is adopted here too. Moreover, it is also supported by the location of the peak in $V(\omega_m)$.

The area of the junctions seemed to have some importance at the 10-μm range but none at all in the 3- and 0.6-μm ranges (junctions with area of 5 μm $\times$ 5 μm led also to similar results). A dc test of junctions with different areas which had been fabricated simultaneously, led us to believe that the tunneling resistivities are related by the ratios of circumferences and not by the ratio of the areas.[25] This suggests that most of the tunneling occurs around the edges of the device, due to the strong fields in the vicinity of the edges. This effect will make the effective area of the large area MOM only a few times larger than in the "Edge MOM." Another possible explanation may raise the question about the validity of the "capacitance" concept at optical frequencies. It is possible that when the frequency increases, the coupled field does not penetrate into the junction and most of the field-assisted tunneling occurs only near the edges (even if one could eliminate the edge effects by some masking procedure).

Coupling efficiencies into the Edge MOM's can be improved; by improving the antennas in the infrared regime or by coupling via guiding in the visible and near-infrared regimes. The SiO_2 buffer layer can serve as a dielectric waveguide (which each junction possesses). Light can be coupled into the waveguide and be guided into the junction with a predicted enhancement of 10-100 in the detected signal, relative to the present situation.

Since oxides can now be grown reproducibly, with thicknesses in the range of the mean free path of hot electrons in them, the new device can be extended into a MOMOM configuration. In this structure, the first junction emits hot electrons, the second collects it, and the common metal is made very thin to minimize collisions of hot electrons in it. A successful operation of MOMOM device will lay the way toward an optical transistor.

[25]Researchers in the past had strong evidence that the edges of evaporated, large-area MOM's enhance conduction through the devices [37], [38].

TABLE I

Ni-NiO-NiO MOM Results. Summary of Experimental Results Using MOM Junctions no. 1 Through 4. Results are Measured at 77 K (10.6 μm) and 120 K (3.39 μm, 0.6328 μm). Junctions no. 3 and 4 Were Fabricated Simultaneously. Results at 3.39 and 0.6328 μm are Heavily Dependent on the Interpolation of the Thermal Signal, so Only the Approximate G is Substituted.

	λ = 10.6μM		λ = 3.39μM		λ = .6328μM	
AREA [μM^2]	3.8	0.06	5.3	0.03	5.3	0.03
Zero Bias Resistivity [Ω]	850	1180	890	8125	890	8125
$S(-I''/I')$ MAX. [1/v]	4.3	3.36	1.72	2.3	1.72	2.3
Calculated Optical Voltage Across the Junction [mV]	10	10	~7	~4.8	~8.4	~6.7
Available Optical Voltage From the Laser [mV]	0.14	0.07	0.22	0.22	0.42	0.44
Enchancement Factor, G	70	150	~15	~15	~15	~15

Acknowledgment

The authors wish to thank Professor S. Schwarz for numerous helpful discussions and advice, C. Slayman for providing numerical estimates on the absorption in the thin films, A. Leasea for the construction of the audio mixer and the biasing current source, R. Hamilton for building the lasers and the cryogenic Dewar, and P. Humphrey for editing and typing the manuscript.

References

[1] J. W. Dees, "Detection and harmonic generation in the submillimeter wavelength region," *Microwave J.*, vol. 9, pp. 48-55, Sept. 1966.

[2] L. O. Hocker, A. Javan, and D. Ramachandra Roo, "Absolute frequency measurement and spectroscopy of gas laser transition in the far infrared," *Appl. Phys. Lett.*, vol. 10, pp. 147-149, Mar. 1967.

[3] L. O. Hocker and A. Javan, "Laser harmonic frequency mixing of two different far infrared laser lines up to 118μ," *Phys. Lett.*, vol. 26A, pp. 255-256, Feb. 1968.

[4] L. O. Hocker, J. G. Small, and A. Javan, "Extension of absolute frequency measurement to the 84μ range," *Phys. Lett.*, vol. 29A, pp. 321-322, June 1969.

[5] K. M. Evenson, J. S. Wells, L. M. Matarrese, and L. B. Elwell,

"Absolute frequency measurements of the 28- and 78-μm CW water vapor laser lines," *Appl. Phys. Lett.*, vol. 16, pp. 159–161, Feb. 1970.

[6] S. I. Green, "Point contact MOM tunneling detector analysis," *J. Appl. Phys.*, vol. 42, pp. 1166–1169, Mar. 1971.

[7] K. M. Evenson, J. S. Wells, and L. M. Matarrese, "Absolute frequency measurement of the CO_2 CW laser at 28 THz (10.6 μm)," *Appl. Phys. Lett.*, vol. 16, pp. 251–253, Mar. 1970.

[8] R. K. Abrams and W. B. Gandrud, "Heterodyne detection of 10.6μ radiation by metal-to-metal point contact diodes," *Appl. Phys. Lett.*, vol. 17, pp. 150–152, Aug. 1970.

[9] B. L. Twu and S. E. Schwarz, "Mechanism and properties of point-contact metal-insulator-metal diode detectors at 10.6μ," *Appl. Phys. Lett.*, vol. 25, pp. 595–598, Nov. 1974.

[10] T. K. Gustafson and T. J. Bridges, "Radiation of difference frequencies produced by mixing in metal-barrier-metal diodes," *Appl. Phys. Lett.*, vol. 25, pp. 56–59, July 1974.

[11] V. Daneu, D. Sokoloff, A. Sanchez, and A. Javan, "Extension of laser harmonic-frequency mixing techniques into the 9μ region with an infrared metal-metal point contact diode," *Appl. Phys. Lett.*, vol. 15, pp. 398–400, Dec. 1969.

[12] D. R. Sokoloff, A. Sanchez, R. M. Osgood and A. Javan, "Extension of laser harmonic-frequency mixing into the 5-μ regions," *Appl. Phys. Lett.*, vol. 17, pp. 257–259, Sept. 1970.

[13] K. M. Evenson, G. W. Day, J. S. Wells, and L. O. Mullen, "Extension of absolute frequency measurements to the CW He–Ne laser at 88 THz (3.39μ)," *Appl. Phys. Lett.*, vol. 20, pp. 133–134, Feb. 1972.

[14] E. Sakuma and K. M. Evenson, "Characteristics of tungsten-nickel point contact diodes used as laser harmonic-generator mixers," *IEEE J. Quantum Electron.*, vol. QE-10, pp. 599–603, Aug. 1974.

[15] D. A. Jennings, F. R. Peterson, and K. M. Evenson, "Extension of absolute frequency measurements to 148 THz: Frequencies of 2.0–and 3.5 μm X_e laser," *Appl. Phys. Lett.*, vol. 26, pp. 510–511, May 1975.

[16] S. M. Faris, T. K. Gustafson, and J. C. Wiesner, "Detection of optical and infrared radiation with dc-biased electron-tunneling metal-barrier-metal diodes," *IEEE J. Quantum Electron.*, vol. QE-9, pp. 737–745, July 1973.

[17] A. Sanchez, S. K. Singh, and A. Javan, "Generation of infrared radiation in a metal-to-metal point-contact diode at synthesized frequencies of incident fields: A high speed broad-band light modulator," *Appl. Phys. Lett.*, vol. 21, pp. 240–243, Sept. 1972.

[18] L. M. Matarrese and K. M. Evenson, "Improved coupling to infrared whisker diodes by use of antenna theory," *Appl. Phys. Lett.*, vol. 17, pp. 8–10, July 1970.

[19] B. L. Twu and S. E. Schwarz, "Properties of infrared cat-whisker antennas near 10.6μ," *Appl. Phys. Lett.*, vol. 26, pp. 672–675, June 1975.

[20] H. D. Riccius, "High frequency limitation of metal-insulator-metal point-contact diodes," *Appl. Phys. Lett.*, vol. 27, pp. 232–233, Aug. 1975.

[21] S. Wang, "Antenna properties and operation of metal-barrier-metal devices in the infrared and visible regions," *Appl. Phys. Lett.*, vol. 28, pp. 303–305, Mar. 1976.

[22] D. P. Siu and T. K. Gustafson, "Coherent coupling of radiation to metal-barrier-metal structures by surface plasmons," *Appl. Phys. Lett.*, to be published.

[23] J. G. Small, G. M. Elchinger, A. Javan, A. Sanchez, F. J. Bachner, and D. L. Smythe, "AC electron tunneling at infrared frequencies: Thin film M-O-M diode structure with broad-band characteristics," *Appl. Phys. Lett.*, vol. 24, pp. 275–279, Mar. 1974.

[24] T. K. Gustafson, R. V. Schmidt, and J. R. Perucca, "Optical detection of thin-film metal-oxide-metal diodes," *Appl. Phys. Lett.*, vol. 24, pp. 620–622, June 1974.

[25] G. M. Elchinger, A. Sanchez, C. F. Davis, Jr., and A. Javan, "Mechanism of detection of radiation in a high-speed metal-metal oxide-metal junction in the visible region and at longer wavelengths," *J. Appl. Phys.*, vol. 47, pp. 591–594, Feb. 1976.

[26] S. Y. Wang, T. Izawa, and T. K. Gustafson, "Coupling characteristics of thin-film metal-oxide-metal diodes at 10.6 μM," *Appl. Phys. Lett.*, vol. 27, pp. 481–483, Nov. 1975.

[27] C. B. Duke, *Tunneling in Solids*. New York: Academic, 1969, chap. 4.

[28] T. E. Hartman, "Tunneling of a wave packet," *J. Appl. Phys.*, vol. 33, pp. 3427–3433, Dec. 1962.

[29] M. Nagae, "Response time of metal-insulator-metal tunnel junctions," *Japan. J. Appl. Phys.*, vol. 11, pp. 1611–1621, Nov. 1972; ——, "Linear response of metal-insulator-metal tunnel junctions to step input voltage," *Japan. J. Appl. Phys.*, vol. 12, pp. 523–530, Apr. 1973.

[30] N. W. Ashcroft and N. D. Mermin, *Solid State Physics*. New York: Holt, Rinehart and Winston, 1976, chap. 1.

[31] Z. Burshtein and J. Levinson, "Photo-induced tunnel currents in Al-Al_2O_3-Au structures," *Phys. Rev. B*, vol. 12, pp. 3453–3457, Oct. 1975.

[32] C. W. Slayman and M. Gudes, to be submitted.

[33] S. R. Pollack and C. E. Morris, "Tunneling through gaseous oxidized film of Al_2O_3," *Trans. Met. Soc. AIME*, vol. 233, pp. 497–501, Mar. 1965. ——, "Electron tunneling through asymmetric films of thermally grown Al_2O_3," *J. Appl. Phys.*, vol. 35, pp. 1503–1512, May 1964.

[34] O. L. Nelson and D. E. Anderson, "Potential barrier parameters in thin-film Al-Al_2O_3-metal diodes," *J. Appl. Phys.*, vol. 37, pp. 77–82, Jan. 1966.

[35] J. H. Greiner, "Josephson tunneling barriers by RF sputter-etching in an oxygen plasma," *J. Appl. Phys.*, vol. 42, pp. 5151–5155, Nov. 1971.

[36] J. Lambe and R. C. Jaklevic, "Molecular vibration spectra by intrinsic electron tunneling," *Phys. Rev.*, vol. 165, pp. 821–832, Jan. 1968.

[37] S. R. Pollack, "Schottky field emission through insulating layers," *J. Appl. Phys.*, vol. 34, pp. 877–880, Apr. 1963.

[38] S. R. Pollack and C. E. Morris, "Electron tunneling through asymmetric films of thermally grown Al_2O_3," *J. Appl. Phys.*, vol. 35, pp. 1503–1512, May 1964.